Catalysis Today 201 (2013) 32–39

Contents lists available at SciVerse ScienceDirect

Catalysis Today

journal homepage: www.elsevier.com/locate/cattod

# A novel redox-precipitation method for the preparation of α-$MnO_2$ with a high surface $Mn^{4+}$ concentration and its activity toward complete catalytic oxidation of *o*-xylene

Yinsu Wu[a], Yao Lu[b], Chaojie Song[c], Zichuan Ma[a,*], Shengtao Xing[a], Yuanzhe Gao[a]

[a] College of Chemistry and Material Science, Hebei Normal University, Shijiazhuang 050024, China
[b] School of Chemistry and Chemical Engineering, Ningxia University, Yinchuan 750021, China
[c] Institute for Fuel Cell Innovation, National Research Council of Canada, Vancouver, BC V6T 1W5, Canada

ARTICLE INFO

*Article history:*
Received 30 December 2011
Received in revised form 22 March 2012
Accepted 1 April 2012
Available online 22 May 2012

*Keywords:*
α-$MnO_2$
High surface concentration of $Mn^{4+}$ ion
Redox-precipitation method
*o*-Xylene
Complete catalytic oxidation

ABSTRACT

A novel redox-precipitation method was developed for the preparation of α-$MnO_2$, where $Mn(NO_3)_2$ and KOH were titrated into excess $KMnO_4$ solution at pH 8. For comparison, $MnO_x$ was also prepared using a conventional precipitation method. These materials were characterized by XRD, BET, SEM/EDS, XPS, and $H_2$-TPR techniques, and their catalytic activities were evaluated for the complete catalytic oxidation of a typical volatile organic compound (VOCs), *o*-xylene. The novel method produced open porous hierarchically structured microcrystalline α-$MnO_2$ containing almost 100% $Mn^{4+}$ ion on its surface. Whereas, the conventional precipitation method produced a mixture of $MnO_2$ and $Mn_3O_4$ with a closely packed spherical morphology containing only 31% $Mn^{4+}$ ion on its surface. It was found that α-$MnO_2$ exhibited good low-temperature reducibility, and that it could convert 100% *o*-xylene into $CO_2$ at 220 °C at a space velocity of 8000 $h^{-1}$, 50 °C lower than the $MnO_x$ prepared by the conventional method. The surface concentration of $Mn^{4+}$ ion in α-$MnO_2$ played a key role for its high catalytic activity for the complete oxidation of *o*-xylene. In addition, the open porous structure and the presence of small amount of potassium ion in the microcrystalline α-$MnO_2$ channel may also be responsible for its excellent catalytic performance. Effects of pH and calcination temperature on its catalytic activity were investigated, and optimal preparation conditions were found. Durability of the α-$MnO_2$ was also studied.



## 1. Introduction

Volatile organic compounds (VOCs) such as benzene, toluene, and xylene (BTX) are harmful to the environment. Therefore, the removal of these pollutants is an important research topic for environmental treatment systems [1,2]. Complete catalytic oxidation techniques that convert an organic compound contaminant into $CO_2$ and $H_2O$ are effective pathways to remove VOCs. Two types of catalysts have been used, alone or in combination, for oxidizing VOCs pollutants: supported noble metals, and transition metal oxides. Although supported precious metals (e.g., Pt and Pd) exhibited high performance at lower temperatures [3–6], the high cost and limited availability restrict their wide application. Thus development of efficient transition-metal-oxide-based catalysts for VOC oxidation has attracted significant interest [7–20].

$MnO_2$ has been considered as an efficient material for redox catalysis because of its polyvalent, novel chemical and physical properties, low cost and environmentally benign features [7,11–13]. Up to now, three types of $MnO_2$ have been used for catalytic combustion of VOCs: pure (bulk) $MnO_2$, supported $MnO_2$, and Mn-containing mixed oxides. For example, Li and co-workers studied $TiO_2$, $Al_2O_3$ and $SiO_2$ supported manganese oxide catalysts for the oxidation of chlorobenzene (1300 ppm). They found that $MnO_x/TiO_2$ (Mn loading, 1.9 wt.%) showed the highest catalytic activity and chlorobenzene was completely oxidized at about 400 °C [13]. Lahousse and co-workers compared the catalytic activities of commercially available γ-$MnO_2$ and $Pt/TiO_2$ for VOC removal and found that γ-$MnO_2$ could catalyze the complete conversion of toluene and methanol at 260 °C, more active than $Pt/TiO_2$ [15].

It is generally accepted that oxidation of hydrocarbons takes place via a redox mechanism in which the rate determining step is oxygen removal from the metal oxide. Thus, the reducibility of metal oxide species and oxygen removal activity appear to be two critical parameters determining their catalytic performance for VOC oxidation [7]. To improve the reducibility and oxygen removal activity of manganese oxide, binary metal oxide catalysts including $MnO_x$-$CeO_2$ oxides, $MnO_x$-$CuO_x$ oxides, $MnO_x$-CoO and $MnO_x$-$ZrO_2$ oxides have been widely studied [11,16–19]. Li et al. investigated

* Corresponding author.
*E-mail address:* ma_zichuan@163.com (Z. Ma).

0920-5861/$ – see front matter © 2012 Elsevier B.V. All rights reserved.
http://dx.doi.org/10.1016/j.cattod.2012.04.032

the catalytic activities of Mn-Cu and Mn-Zr mixed oxides prepared by a reverse microemulsion method. The Cu-Mn catalyst showed higher activity for complete oxidation of toluene. $Mn_{0.67}$-$Cu_{0.33}$ (Cu loading 33 mol%) could catalyze the complete oxidation of toluene (0.35 vol.%) at about 220 °C [11]. Recently, our group studied the catalytic performance of $MnO_x$-$CeO_2$ oxides prepared by a redox-precipitation method, and found that the $MnO_x$-$CeO_2$ catalyst could catalyze the conversion of *o*-xylene (0.05 vol. %) into $CO_2$ and $H_2O$ at 240 °C [19]. We found that $MnO_2$ is the main active phase providing the oxygen species, and that $CeO_2$ enhanced the oxygen mobility. The synergistic effects between $MnO_2$ and $CeO_2$ promoted the redox behavior of the catalyst and significantly improved its activity toward the complete catalytic oxidation of *o*-xylene [19].

The reducibility of pure $MnO_x$ is dependent on its oxidation state and morphology. Generally speaking, Mn ion with high oxidation state may have high redox activity in which Mn ion is partially reduced by donating oxygen, and then the reduced Mn ion is reoxidized via the intake of oxygen from the gas phase [21]. Thus, $MnO_x$ containing high content $Mn^{4+}$ ion may exhibit higher catalytic performance. In addition, porous, hierarchically nanostructured materials are potentially good candidates for next generation high-performance catalysts, because of their high surface area and open porous structure, both of which facilitate gas diffusion and adsorption [21]. According to our previous study, hierarchically structured $MnO_2$ could be prepared by controlling the precipitation kinetics and precursor adsorption in the redox reaction between $Mn^{2+}$ ions and $KMnO_4$ in an acidic medium at room temperature without any templates [22]. However, this hierarchical structure consists of $MnO_2$ in loose aggregates, and has poor thermal stability, which is not applicable to complete catalytic oxidation of VOCs. It was reported that a certain amount of $K^+$ ion could prevent the α-$MnO_2$ tunnels from collapsing during the heating process [20,23].

It is also known that besides $Mn^{4+}$ ion, there co-exist $Mn^{3+}$ and $Mn^{2+}$ ions in $MnO_x$. However, so far few studies have focused on the relationship between the surface $Mn^{4+}$ concentration and its catalytic activity toward VOCs catalytic oxidation. Also, by now, complete BTX oxidation catalyzed by pure $MnO_x$ can only be achieved at temperatures above 240 °C [15,23]. It remains a big challenge to prepare $MnO_x$ that can lower down the combustion temperature of VOCs.

In this paper, a new redox-precipitation method was developed to synthesize hierarchically structured α-$MnO_2$ with almost 100% $Mn^{4+}$ ion, where $Mn(NO_3)_2$ and KOH were added into excess $KMnO_4$ solution at pH 8. For comparison, a $MnO_x$ catalyst containing $Mn^{4+}$, $Mn^{3+}$, and $Mn^{2+}$ ions was also prepared via a conventional precipitation method. The two catalysts were tested for the complete catalytic oxidation of *o*-xylene. The effects of the surface $Mn^{4+}$ concentration in $MnO_x$ and morphology on their catalytic activity toward VOCs catalytic combustion were investigated. Other factors such as pH and calcination temperature were also optimized for this novel redox-precipitation method.

## 2. Experimental

### 2.1. Catalyst preparation

All the chemical reagents were of analytical pure grade and used as received. The new redox-precipitation route was as follows, a calculated amount of $KMnO_4$ precursor, in 10% stoichiometric excess, was dissolved in deionized water. The solution was kept at 60 °C titrated with 50% $Mn(NO_3)_2$ solution under vigorous stirring. The pH of the mixture was kept constant at a value of 6.0, 8.0, and $10.0 \pm 0.3$ respectively by the addition of 0.2 M KOH solution. The precipitate was aged for 2 h at 60 °C, and then filtered, washed with distilled water and dried overnight at 100 °C. The dried samples were calcined in air at 350–600 °C for 6 h. The catalyst was denoted as RP-$MnO_x$ (*Y*–*Z*), where *Y* is pH value and *Z* represents the calcination temperature in °C.

For comparison, a $MnO_x$ catalyst was also prepared via a conventional precipitation method. Typically, 0.2 M KOH solution was added dropwise to $Mn(NO_3)_2$ solution under vigorous stirring at 60 °C. The pH of the mixture was kept at 8.0, The precipitate was aged for 2 h at 60 °C, and then filtered, washed with distilled water and dried overnight at 100 °C. The dried sample was calcined in air at 400 °C for 6 h. This catalyst was denoted as CP-$MnO_x$ (8-400).

### 2.2. Catalyst characterization

The catalysts were characterized using $N_2$ adsorption/desorption isotherm, X-ray diffraction (XRD), X-ray photoelectron spectroscopy (XPS), Scanning electron micrographs (SEM) and Energy dispersive X-ray (EDS). The nitrogen adsorption–desorption isotherm was obtained at −196 °C using a Quantachrome Autosorb-1c instrument. Before measurement, the samples were degassed at 300 °C for 4 h. The surface area was calculated from the isotherms according to the BET method, and the average pore size was calculated using the BJH method. XRD was performed in the $2\theta$ range of 20–80° with a step size of 0.05°/s using a D8-ADVANCE diffractometer (Germany) operated at 40 kV and 40 mA with a nickel-filtered Cu Kα ($\lambda = 0.15418$ nm) nmradiation source. XPS spectra were obtained using a SHIMADZU ESCA-3400 spectrometer (Mg Kα radiation). The binding energy regions investigated were 280–300 eV (C1s), 522–542 eV (O1s), and 630–670 eV (Mn 2p) using a C1s line (284.8 eV) of adventitious carbon as a reference. SEM and EDS were taken on a Hitachi, S-4800 microscope. Before the SEM and EDS tests, the powder samples were spread uniformly on carbon paste on a copper holder and then coated with gold.

### 2.3. $H_2$-TPR

Temperature programmed reduction (TPR) experiments were performed from room temperature up to 600°C under a flow of 5% $H_2$/Ar mixture (30 mL $min^{-1}$) over 30 mg of catalyst at a heating rate of 10 °C $min^{-1}$. Prior to the TPR experiments, the catalysts were pretreated in a 20% $O_2$/He mixture at 400°C for 1 h to clean the surface of the catalysts. A mass spectrometer (Hiden HPR20) was used for on-line monitoring of the TPR effluent gas.

### 2.4. Catalytic activity measurement

Catalytic activity was measured in a 4 mm i.d. quartz tubular reactor. 0.25 g of catalyst supported by quartz wool was placed in the middle of the reactor. A gas containing 700 ppm *o*-xylene in simulated air (20 vol.% $O_2$, 80 vol.% $N_2$) continuously passed through the catalyst bed with a flow rate of 50 mL $min^{-1}$ and $W/F = 0.3$ g s $mL^{-1}$ (corresponding to a GHSV of 8000 $h^{-1}$). Here, $W/F$ is defined as the catalyst weight divided by the gas flow rate. $CO_2$ was the only detectable C-containing reaction product, which passed through the TDX-01 stainless steel packed column firstly, and was then converted into methane in a reformer furnace. No significant amount of any partial oxidation product was detected in the effluent. The reactant and reaction product were analyzed with an on-line gas chromatograph equipped with two flame ionization detectors (FID) in series. *o*-Xylene conversion ($X_{o\text{-xylene}}$) and the yield of $CO_2$ ($Y_{CO_2}$) were calculated according to the following equations:

$$X_{o\text{-xylene}} = 100 \times \frac{(o\text{-xylene}_{in} - o\text{-xylene}_{out})}{o\text{-xylene}_{in}} \quad (1)$$

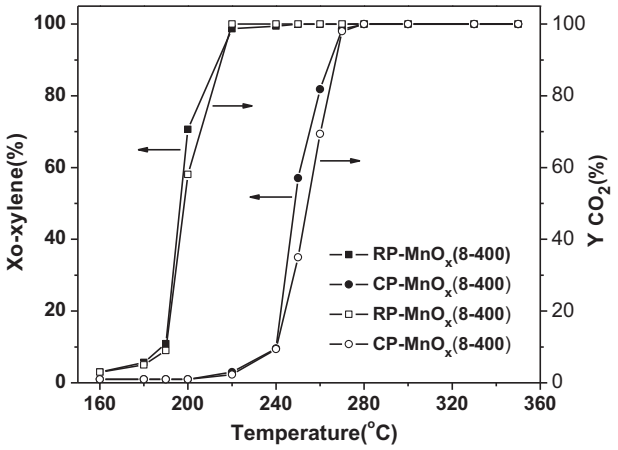


**Fig. 1.** *o*-Xylene conversion and $CO_2$ yield over RP-$MnO_x$ (8-400) and CP-$MnO_x$ (8-400) catalysts. Reaction conditions: *o*-xylene 700 ppm, 20% $O_2/N_2$ balance, total flow rate 50 mL $min^{-1}$, $W/F = 0.30$ g s $mL^{-1}$.

$$Y_{CO_2} = \frac{100 \times CO_{2\,out}/8}{o\text{-xylene}_{in}} \quad (2)$$

## 3. Results and discussion

### 3.1. Effect of preparation method

Fig. 1 shows *o*-xylene conversion and $CO_2$ yield versus temperature over RP-$MnO_x$ (8-400) and CP-$MnO_x$ (8-400). The result indicates that *o*-xylene conversion and $CO_2$ yield were temperature dependent and were significantly affected by the catalyst preparation method. The RP-$MnO_x$ (8-400) catalyst showed 100% of *o*-xylene conversion and $CO_2$ yield at 220 °C while the CP-$MnO_x$ (8-400) catalyst exhibited the same conversion efficiency and $CO_2$ yield at 270 °C, 50 °C higher than the RP-$MnO_x$ (8-400) catalyst, indicating that RP-$MnO_x$ (8-400) had higher catalytic activity than CP-$MnO_x$ (8-400). For CP-$MnO_x$ (8-400), there is a gap between the *o*-xylene conversion and $CO_2$ yield at 240–270 °C. Whereas for RP-$MnO_x$ (8-400), this gap is not as significant as that observed with CP-$MnO_x$ (8-400). These results indicate that RP-$MnO_x$ (8-400) exhibit excellent catalytic activity for the complete catalytic oxidation of *o*-xylene.

The XRD patterns of RP-$MnO_x$ (8-400) and CP-$MnO_x$ (8-400) are shown in Fig. 2. On CP-$MnO_x$ (8-400), typical diffraction peaks of $Mn_3O_4$ were observed at 2$\theta$ of 28.7°, 30.9°, 32.3°, 36.2°, 38.3°, 44.3°, 50.8°, 58.2°, 60.0° and 64.7° (PDF #43-1002), and very weak diffraction peaks of $MnO_2$ were observed at 37.1°, 47.8°, 55.9° and

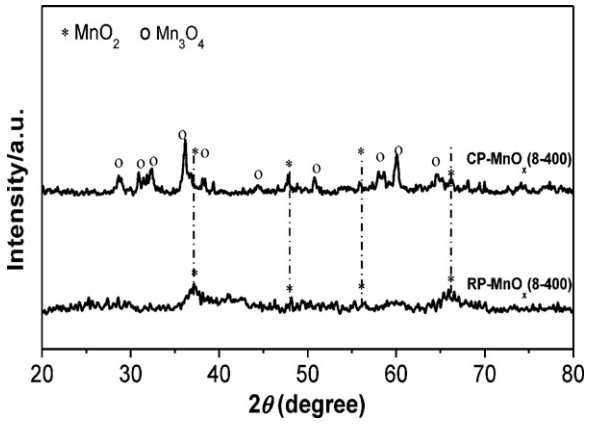


**Fig. 2.** XRD patterns of RP-$MnO_x$ (8-400) and CP-$MnO_x$ (8-400).

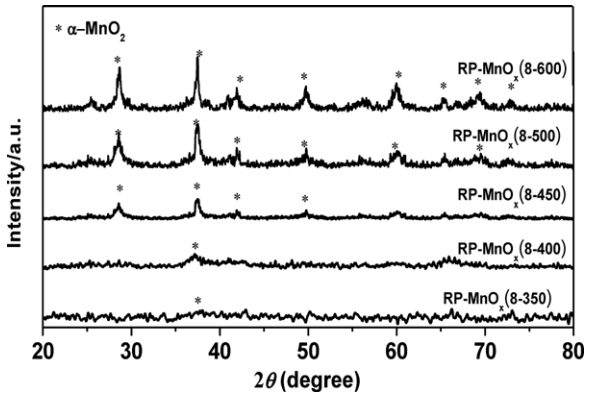


**Fig. 3.** XRD patterns of RP-$MnO_x$ after heat treatment at varied temperatures of 350–600 °C.

66.2°. For RP-$MnO_x$ (8-400), two weak, broad peaks in the 2$\theta$ range of 35–40° and 65–70° were observed. In order to determine the phase composition of RP-$MnO_x$ (8-400), the as-prepared RP-$MnO_x$ (8-*Z*) was calcined at 350 °C up to 600 °C (see Fig. 3). The crystalinity increases as the heat treatment temperature increase. RP-$MnO_x$ (8-350) showed completely amorphous phase, which may be a mixture of manganese oxide and manganese salts. As the calcination temperature increased to 500 °C, relativity sharp diffraction peaks at $2\theta = 28.6°, 37.4°, 41.8°, 49.7°, 60.1°$ and 69.4° appeared, which are typical diffraction lines of α-$MnO_2$ (JCPDS44-0141). When the sample was further heated to 600 °C, the intensities of these α-$MnO_2$ peaks enhanced, indicating an increase in degree of crystallization and crystallite size. It is reasonable to postulate that RP-$MnO_x$ (8-400) was composed of microcrystalline structured α-$MnO_2$. These results also illustrate that the new redox-precipitation method produces pure α-$MnO_2$. Moreover, this α-$MnO_2$ exhibits high phase stability up to 600 °C.

The BET surface area and pore volume of RP-$MnO_x$ (8-400) are 69.42 $m^2\,g^{-1}$ and 0.51 $cm^3\,g^{-1}$, respectively, significantly larger than those of CP-$MnO_x$ (8-400) (23.20 $m^2\,g^{-1}$ and 0.25 $cm^3\,g^{-1}$). However, the pore size of RP-$MnO_x$ (8-400) is only 29.51 nm, significantly smaller than that of CP-$MnO_x$ (8-400) (43.29 nm). These results indicate that the preparation method greatly affects the physical properties of these catalysts.

Further insight into the influence of preparation method on the structural features of the catalysts came from SEM images of the RP-$MnO_x$ and CP-$MnO_x$ samples before and after calcination at 400 °C (Fig. 4A–D). The texture and morphology of the as-prepared RP-$MnO_x$ are significantly different from that after calcination at 400 °C. The as-prepared RP-$MnO_x$ consists of a series of nanosheets assembled into nanoflower shape with diameters of 300-500 nm. These nanosheets interweave together forming open porous structure in the nanoflowers (Fig. 4A). After calcination (RP-$MnO_x$ (8-400)), most of these nanosheets disappear, converting the nanoflowers into porous nanospheres. In some of the nanoflowers, the nanosheets agglomerate into larger petal-like sheets, and the nanoflowers agglomerate into larger flower shaped particles, as shown in Fig. 4B. No significant morphological change was observed with CP-$MnO_x$ samples before (Fig. 4C) and after (Fig. 4D) calcination. The as-prepared CP-$MnO_x$ consists of large and closely packed spherical particles with particle size of 200–500 nm and irregularly shaped particles. After calcination at 400 °C (CP-$MnO_x$ (8-400)), these particles almost did not change. Fig. 4E and F shows that the EDS spectra of the as-prepared RP-$MnO_x$ and CP-$MnO_x$, revealing that the as-prepared CP-$MnO_x$ is composed of only Mn and O, whereas the RP-$MnO_x$, consisted of Mn, O, as well as K.

The XRD and SEM results indicate that the composition and morphology of $MnO_x$ are dependent on the reaction method. In the

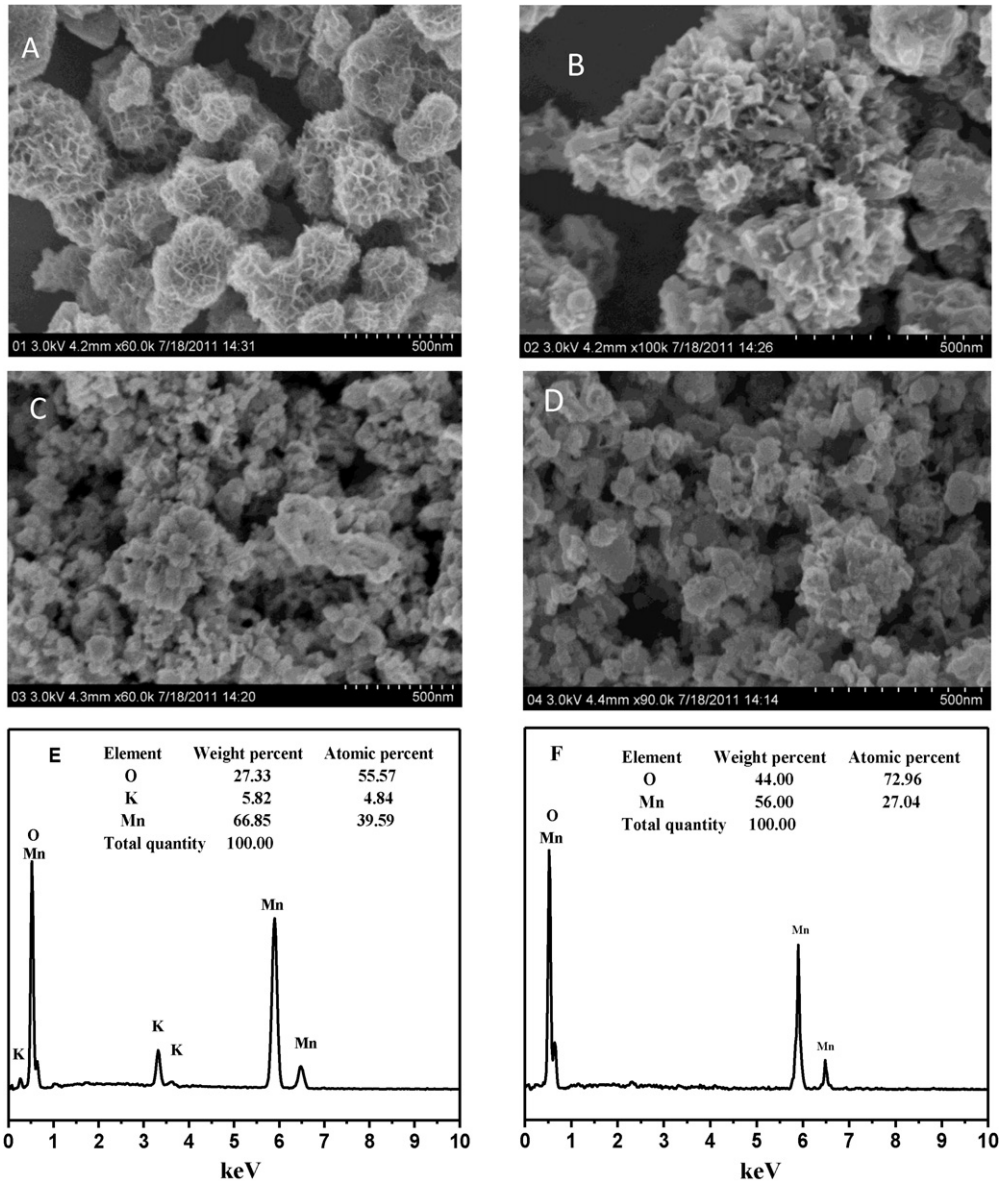


**Fig. 4.** SEM images (A–D) of RP-$MnO_x$ and CP-$MnO_x$ samples; for RP-$MnO_x$ before and after calcination at 400 °C (A–B); for CP-$MnO_x$ before and after calcination at 400 °C (C–D); EDS (E) patterns of RP-$MnO_x$ (8-400); EDS (F) patterns of CP-$MnO_x$ (8-400).

conventional precipitation method, dissolved oxygen is the only oxidizer in the solution, a mixture of $Mn(OH)_2$ and $MnO_x$ might form quickly, which may grow and agglomerate to form large, dense spherical particles. After calcination, the mixture was converted into $Mn_3O_4$ and $MnO_2$. In the redox precipitation method, $MnO_2$ was mainly produced because of the presence of powerful oxidant $MnO_4^-$. In our previous study, we have found that the desired crystal morphologies can be obtained by manipulating the precursor adsorption [22]. In the present redox-precipitation process, when $Mn^{2+}$ was dripped into the $MnO_4^-$ solution at pH 8, the initially formed $MnO_2$ was negatively charged. The following added $Mn^{2+}$ might be preferentially adsorbed on the most favored lattice face, along which direction it reacted with $MnO_4^-$. Due to the anisotropic effect, nanosheets were formed. Then, the nanosheets assembled into nanoflowers with diameters of 200–500 nm.

The $H_2$-TPR profiles of the RP-$MnO_x$ (8-400) and CP-$MnO_x$ (8-400) samples are shown in Fig. 5. It can be seen that the reduction behaviors strongly depended on the preparation method. The $H_2$-TPR profile of the CP-$MnO_x$ (8-400) sample exhibited a weak

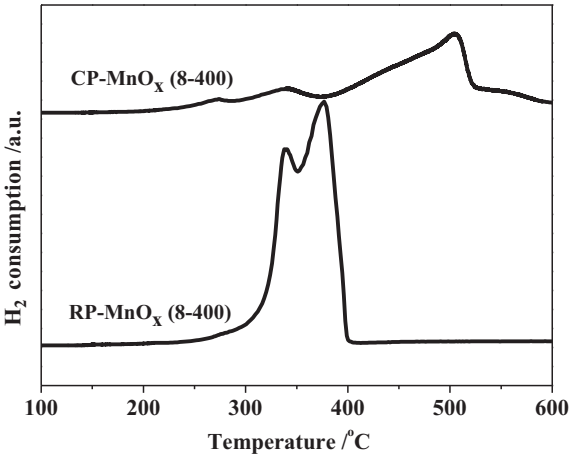


**Fig. 5.** $H_2$-TPR profiles of RP-$MnO_x$ (8-400) and CP-$MnO_x$ (8-400).

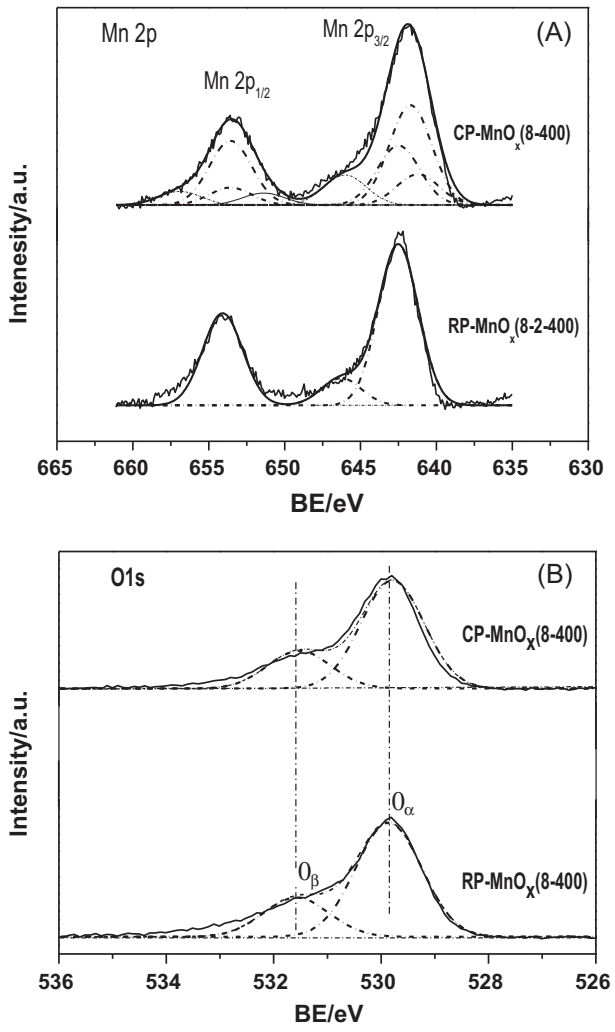


**Fig. 6.** Mn 2p XPS spectra (A) and O1s XPS spectra (B) of RP-$MnO_x$ (8-400) and CP-$MnO_x$ (8-400).

reduction peak around 340 °C, followed by a broad moderate intensity reduction peak with a maximum at 505 °C. Whereas, two intensive reduction peaks centered at lower temperatures of 338 °C and 377 °C were observed for the RP-$MnO_x$ (8-400) sample. In general, the low temperature reduction could be assigned to the reduction of $MnO_2$ to $Mn_3O_4$, and the high-temperature reduction corresponded to the reduction of $Mn_3O_4$ to MnO [23–25]. Moreover, it can be seen that the amount of consumed hydrogen over the RP-$MnO_x$ (8-400) sample was much high than that of the CP-$MnO_x$ (8-400) sample. Whereas, the reduction temperature of RP-$MnO_x$ (8-400) was extremely lower than that of CP-$MnO_x$ (8-400). TPR analyses showed that the redox behavior of the manganese oxide in RP-$MnO_x$ (8-400) was potentiated, indicating improved oxygen mobility and availability. The RP-$MnO_x$ (8-400) exhibited good low-temperature reducibility, which may also be responsible for its high catalytic activity in the complete oxidation of *o*-xylene.

To measure the composition and oxidation state of RP-$MnO_x$ (8-400) and CP-$MnO_x$ (8-400), XPS spectra were taken on the two samples, as shown in Fig. 6(A) shows the XPS spectra of Mn 2p in RP-$MnO_x$ (8-400) and CP-$MnO_x$ (8-400). RP-$MnO_x$ (8-400) showed a sharp, strong Mn 2p peak at 642.4 eV, attributed to $Mn^{4+}$ (641.1–642.4 eV) in $MnO_2$ [26], indicating $MnO_2$ species was formed on the RP-$MnO_x$ (8-400). The sharpening of this XPS peak may be attributed to the stabilization of only one type of manganese oxide [27], in agreement with the XRD result. Furthermore, the intense signal at 642.4 eV indicates that there was a high surface atomic concentration of $Mn^{4+}$ in the RP-$MnO_x$ (8-400). For the CP-$MnO_x$ (8-400), a broad, strong Mn 2p peak was observed, suggesting Mn ion exists as more than one oxidation state [19,27]. As discussed above, the XRD and TPR results indicated two types of manganese oxide existed in CP-$MnO_x$ (8-400). Satellite peaks were also observed with RP-$MnO_x$ (8-400) and CP-$MnO_x$ (8-400) at 646.0–647.0 eV, which likely originated from the charge transfer between the outer electron shell of the ligand and the unfilled 3d shell of Mn during the creation of the core-hole in the photoelectron process [27]. Table 1 summarizes the surface compositions of $Mn^{4+}$ in RP-$MnO_x$ (8-400) and CP-$MnO_x$ (8-400), calculated from the XPS spectra. RP-$MnO_x$ (8-400) possessed 100% $Mn^{4+}$ ions, whereas CP-$MnO_x$ (8-400) only has and 31%. Table 1 also demonstrated that in CP-$MnO_x$ (8-400) Mn exists as $Mn^{4+}$, $Mn^{3+}$, and $Mn^{2+}$. Machocki et al. reported that high $Mn^{4+}$ concentration is beneficial for the catalytic combustion of hydrocarbons [28]. By comparing the catalytic performance of RP-$MnO_x$ (8-400) and CP-$MnO_x$ (8-400) with their surface $Mn^{4+}$ ions content, one can see that the catalytic activity is correlated with the surface $Mn^{4+}$ ion content, which means that the large amount of $Mn^{4+}$ species on the surface of RP-$MnO_x$ (8-400) may account for its high activity and selectivity during the complete catalytic oxidation of *o*-xylene.

The O1s spectrum is frequently used to identify the types of surface oxygen species present in a particular oxide. The chemical environment of oxygen in metal oxide catalysts played an important role in their catalytic properties. Fig. 6(B) shows the XPS spectra of O1s in RP-$MnO_x$ (8-400) and CP-$MnO_x$ (8-400). For both materials, three peaks were observed, attributing to three types of oxygen species: the peak at BE of 529–530 eV was ascribed to the lattice oxygen (denoted as $O_\alpha$), the peak at BE of 531–532 eV was ascribed to defective oxides or surface oxygen ions with low coordination (denoted as $O_\beta$) [19,27], and the peak at a higher BE (above 533 eV) corresponded to adsorbed water [26]. Peak deconvolution was only performed for the $O_\alpha$ and $O_\beta$ species, because the adsorbed water peak was too weak [26]. The relative amounts of $O_\alpha$ in RP-$MnO_x$ (8-400) and CP-$MnO_x$ (8-400) are almost the same, 74.2% for CP-$MnO_x$ (8-400), and 74.5% for RP-$MnO_x$ (8-400) (see Table 1). However, the $H_2$-TPR results showed that the oxygen specie on RP-$MnO_x$ (8-400) was more active than that of CP-$MnO_x$ (8-400).

The oxidation of organic molecules over metal oxide catalysts usually proceeds according to the Mars and Van Krevelen (MVK) mechanism [29], where the organic molecules is oxidized by the lattice oxygen of the metal oxide, the latter being re-oxidized by gas phase oxygen in the feed gas. Therefore, the reducibility of metal oxide species and oxygen removal activity appear to be two critical parameters determining their catalytic performance for VOC oxidation.

Higher oxidation state of manganese species was previously found to be preferable for oxidation reactions over the manganese-containing catalysts. Machocki et al. [28] reported that the rate of methane oxidation over $LaMnO_3$ displays a linear relationship with the surface $Mn^{4+}/Mn^{3+}$ ratio. Park et al. [30] also reached the same conclusion that $PdO_x/MnO_2$ catalyst showed higher catalytic activity for CO oxidation than $PdO_x/Mn_2O_3$ in their comparative study of the support effect between $MnO_2$ and $Mn_2O_3$. Similar phenomenon was observed in the present study, and the RP-$MnO_x$ (8-400) catalyst that possessed almost 100% $Mn^{4+}$ species and richer lattice oxygen species resulted in much higher catalytic activity for the complete oxidation of *o*-xylene. Combined the analysis of above characterizations, we deduced that the high surface $Mn^{4+}$ concentration resulted in high lattice oxygen content, high surface area, and open porous structure of RP-$MnO_x$ (8-400), which may provide more active sites and facilitate the adsorption and diffusion of reactant molecules, resulting in fast oxygen diffusion and enhanced mobility of lattice oxygen. Moreover, the presence of small amount

**Table 1**
XPS results of RP-$MnO_x$ (8-400) and CP-$MnO_x$ (8-400).

| Sample | BE (eV) | | | $Mn^{4+}/(Mn^{4+}+Mn^{3+}+Mn^{2+})$ (%) | BE (eV) | | $O_\alpha/(O_\alpha+O_\beta)$ (%) |
|---|---|---|---|---|---|---|---|
| | $Mn^{4+}$ | $Mn^{3+}$ | $Mn^{2+}$ | | $O_\alpha$ | $O_\beta$ | |
| CP-$MnO_x$ (8-400) | 642.4 | 641.7 | 641.2 | 31.26 | 529.8 | 531.5 | 74.2 |
| RP-$MnO_x$ (8-400) | 642.4 | – | – | 100 | 529.9 | 531.6 | 74.5 |

of potassium ion in the microcrystalline α-$MnO_2$ may weaken the Mn—O bond and improve the reducibility of RP-$MnO_x$ (8-400) [20], thus enhancing its catalytic activity.

### 3.2. Effect of the pH value

It was reported that the pH value played important roles in determining the crystal structures and morphology of final products [31]. In our previous experiments, we found that the $MnO_x$ synthesized via mixing $KMnO_4$ and $Mn(NO_3)_2$ in acidic media (pH < 5) was not thermally stable and could not be used as gas-phase catalysts. High pH may lead to the formation of $Mn(OH)_2$. Thus pH values between 6 and 10 were used in this work. Since $K^+$ ions can stabilize $MnO_x$ structure, KOH was used as base reagent to adjust the pH.

Fig. 7 shows the *o*-xylene conversion and $CO_2$ yield over RP-$MnO_x$ (*Y*-400) catalysts prepared at pH 6, 8, and 10, and calcined at 400 °C. Above 220 °C, all three catalysts exhibited similar catalytic activities for *o*-xylene removal, and 100% conversion of *o*-xylene was achieved. The RP-$MnO_x$ (*Y*-400) prepared at pH 8 showed significantly higher *o*-xylene conversion efficiency than the others at 200 °C. Similar phenomena were observed with the $CO_2$ yield.

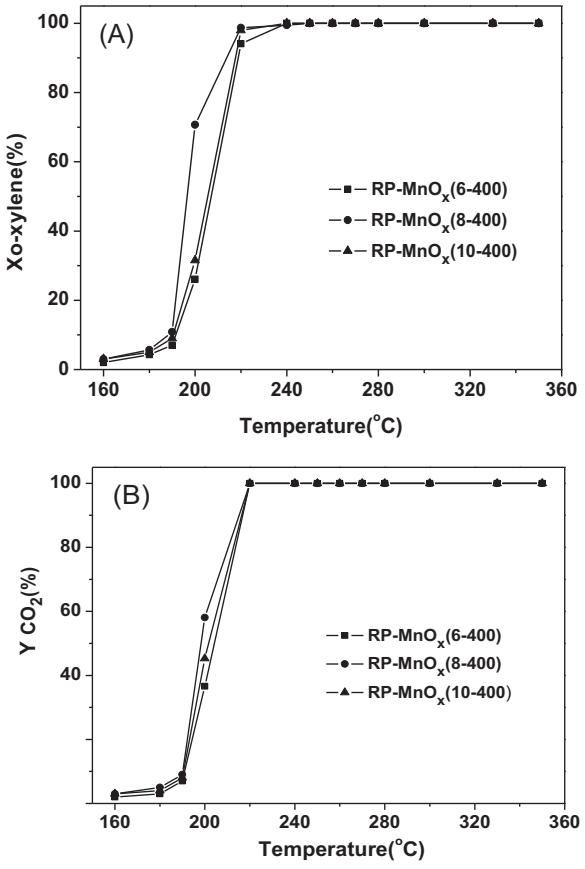


**Fig. 7.** Effect of pH value on *o*-xylene conversion (A) and $CO_2$ yield (B) over RP-$MnO_x$ (*Y*-400) samples. Reaction conditions: *o*-xylene 700 ppm, 20% $O_2/N_2$ balance, total flow rate 50 mL $min^{-1}$, $W/F = 0.30$ g s $mL^{-1}$.

Above 220 °C, all three catalysts gave 100% $CO_2$ yield. Significant difference in $CO_2$ yields was observed between 180 and 200 °C. $T_{50}$ (the temperature needed to reach a $CO_2$ yield of 50%) was usually used to measure the catalytic activity in terms of $CO_2$ yield. The $T_{50}$ of RP-$MnO_x$ (8-400) was found to be 192 °C, whereas the $T_{50}$ of RP-$MnO_x$ (6-400) and RP-$MnO_x$ (10-400) was 206 °C and 204 °C respectively. These results suggest that the catalytic activity is dependent on the pH value, and that pH 8 is the optimal value.

The XRD patterns of the RP-$MnO_x$ (*Y*-400) (*Y* = 6, 8, 10) samples are presented in Fig. 8. All three RP-$MnO_x$ (*Y*-400) catalysts showed similar XRD patterns. As discussed above, for RP-$MnO_x$ (8-400), the diffraction peaks observed in $2\theta$ ranges of 35–40° and 65–70° were attributed microcrystalline α-$MnO_2$ active phase. Compared with RP-$MnO_x$ (8-400), RP-$MnO_x$ (6-400) exhibited three stronger diffraction peaks at $2\theta = 28.5°$, 37.5°and 49.6°, also attributed to α-$MnO_2$. However, the RP-$MnO_x$ (10-400) only showed one weak peak at $2\theta = 37.5°$. At pH 6, the reaction system was a weak acidic solution, the reaction between $KMnO_4$ and $Mn(NO_3)_2$ is relatively rapid due to the distinguishing redox potential of $MnO_4/MnO_2$ (1.70) and $MnO_2/Mn^{2+}$ (1.23), which might produce a product with high crystalinity, displaying strong diffraction peaks. While at pH 10, the reaction condition is milder, and the formation of $MnO_2$ might be slower than that at pH 8. Also $Mn(OH)_2$ may be produced from this basic system, resulting in the formation of an amorphous phase. Most possibly, the product with a certain degree of crystallinity might exhibit high catalyst activity, as observed with RP-$MnO_x$ (8-400).

### 3.3. Effect of calcination temperature

Calcination may change a catalyst's morphology and further affect its catalytic activity. Thus effect of calcination temperature on the catalytic activity of RP-$MnO_x$ (8-*Z*) was investigated for the catalytic oxidation of *o*-xylene. Fig. 9 shows the catalytic activities of RP-$MnO_x$ (8-Z) catalysts that were calcined at 350–600 °C. As the calcination temperature increased from 350 °C to 400 °C, the *o*-xylene conversion and $CO_2$ yield increased slightly, after that, further increase to 500 °C resulted in a catalytic activity decrease, as evidenced from their $T_{50}$ values (208 °C, 196 °C, and 201 °C for RP-$MnO_x$ (8-350), RP-$MnO_x$ (8-400) and RP-$MnO_x$ (8-500) respectively), to the material calcined at 600 °C, showed an extremely low catalytic activity.

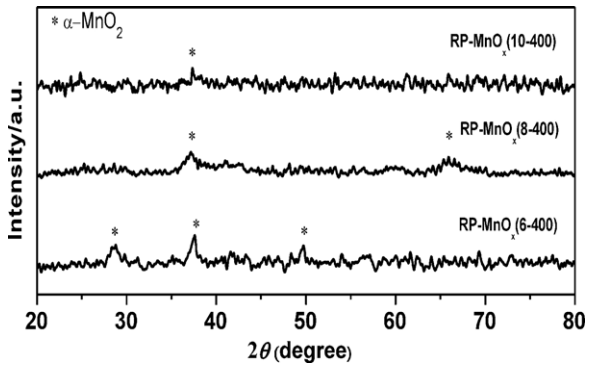


**Fig. 8.** XRD patterns of RP-$MnO_x$ (*Y*-400) samples at varied pH of 6–10.

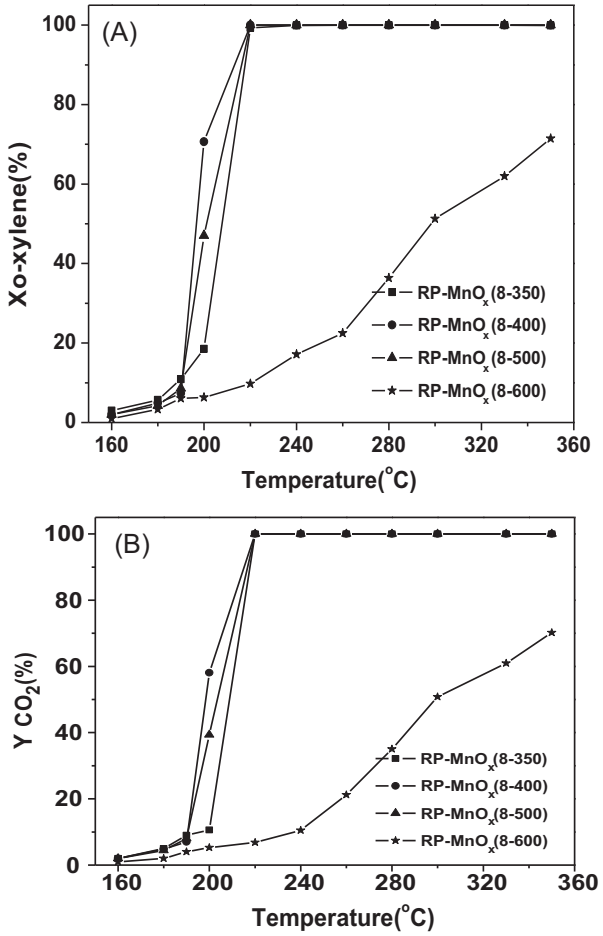


**Fig. 9.** Effect of calcination temperature on *o*-xylene conversion (A) and $CO_2$ yield (B) over RP-$MnO_x$ (8-*Z*) samples. Reaction conditions: *o*-xylene 700 ppm, 20% $O_2/N_2$ balance, total flow rate 50 mL $min^{-1}$, $W/F = 0.30$ g s $mL^{-1}$.

High calcination temperature may result in the formation of larger degree of crystallinity and larger crystal size, as evidenced in Fig. 3. High calcination temperature may also lead to a decrease in reducibility of $MnO_2$ and low BET surface area. Fig. 10 shows the TPR profiles of the RP-$MnO_x$ (8-*Z*) (*Z* = 400, 500, 600). For the samples calcined at 400 °C and 500 °C, two reduction peaks located at about 338 °C, 350 °C and 377 °C, 386 °C, respectively, can be clearly observed. As discussed above, the low temperature reduction peak

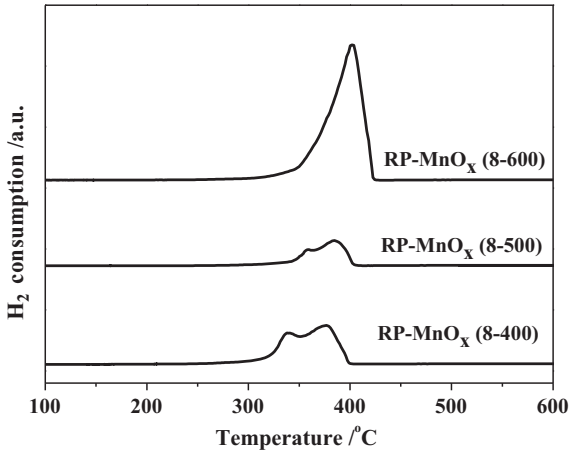


**Fig. 10.** $H_2$-TPR profiles of RP-$MnO_x$ (8-*Z*) samples.

**Table 2**
BET surface area and activity of RP-$MnO_x$ (8-*Z*) for the catalytic oxidation of *o*-xylene at 190 °C.

| Catalysts | Surface area ($m^2\ g^{-1}$) | Conversion[a] at 190 °C (%) | Areal rate[b] (mol $m^{-2}\ min^{-1}$) |
|---|---|---|---|
| RP-$MnO_x$ (8-350) | 60.31 | 7.32 | $3.39 \times 10^{-9}$ |
| RP-$MnO_x$ (8-400) | 69.42 | 10.77 | $4.33 \times 10^{-9}$ |
| RP-$MnO_x$ (8-500) | 57.29 | 8.58 | $4.18 \times 10^{-9}$ |
| RP-$MnO_x$ (8-600) | 43.15 | 6.10 | $3.94 \times 10^{-9}$ |

[a] Reaction rate was determined under the conditions which obtained a *o*-xylene conversion level of below 30%.
[b] Areal rate = $[o\text{-xylene}]_{in}$ × rate of flow × conversion/surface area.

could be attributed to the reduction of $MnO_2$ to $Mn_3O_4$, and the high-temperature reduction peak was assigned to the reduction of $Mn_3O_4$ to MnO. However, the two reduction peaks integrated into single reduction peak and shifted to higher temperatures with increasing the calcination temperature up to 600 °C, indicating the reducibility of $MnO_2$ decreased as calcination temperature increased, which also contribute to their corresponding catalytic activity decrease.

Table 2 summarized the surface area and catalytic activity over RP-$MnO_x$ (8-*Z*) (*Z* = 350, 400, 500, and 600) at 190 °C. The areal rate reflects the intrinsic activity of catalyst, calculated from the conversion efficiency of *o*-xylene and BET surface area. For RP-$MnO_x$ (8-*Z*) (*Z* = 400, 500, and 600), increase in calcination temperature leads to BET surface area decrease, and their catalytic activity decreased correspondingly. The RP-$MnO_x$ (8-350) has a higher BET surface area than RP-$MnO_x$ (8-500) and RP-$MnO_x$ (8-600). However its catalytic activity is lower than the other two. This is possibly due to its amorphous $MnO_x$ phase. The catalyst with a certain degree of crystallinity showed high catalytic activity. The highest catalytic activity was observed with RP-$MnO_x$ (8-400), which has the largest BET surface area and an optimal degree of crystallinity.

The RP-$MnO_x$ (8-*Z*) (*Z* = 400, 500, 600) catalysts have similar areal rates as shown in Table 2, suggesting that these catalysts have the similar catalytic active center, namely, α-$MnO_2$. The areal rate of RP-$MnO_x$ (8-350) at 190 °C was smaller than that of RP-$MnO_x$ (8-400), illustrating that that the active center of α-$MnO_2$ was not completely formed in RP-$MnO_x$ (8-350).

### 3.4. Stability test for the RP-$MnO_x$ (8-400) catalyst

The stability of RP-$MnO_x$ (8-400) was tested for the isothermal combustion of *o*-xylene at 220 °C for 60 h. Fig. 11 shows

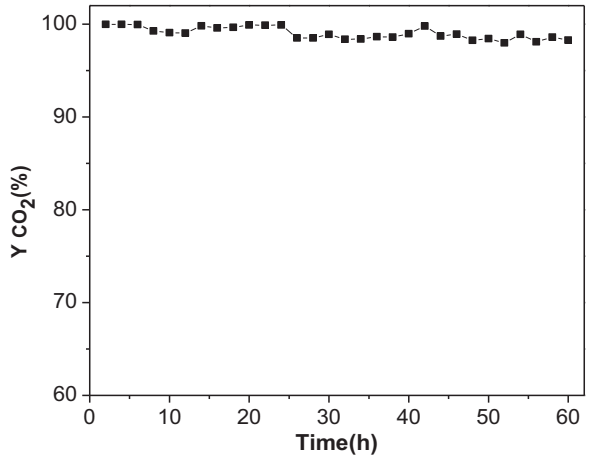


**Fig. 11.** $CO_2$ yield versus on stream time over the RP-$MnO_x$ (8-400) catalyst. Reaction conditions: *o*-xylene 700 ppm, 20% $O_2/N_2$ balance, total flow rate 50 mL $min^{-1}$, $W/F = 0.30$ g s $mL^{-1}$.

the result. $CO_2$ yield remained >98% during the test, indicating. RP-$MnO_x$ (8-400) is relatively stable under these working conditions.

## 4. Conclusion

A new redox-precipitation method followed by calcination at 400 °C was developed, and open porous hierarchically structured α-$MnO_2$, was prepared. The physicochemical properties of the materials were characterized by the XRD, BET, SEM/EDS, XPS, and $H_2$-TPR techniques, and the catalytic activity was tested for *o*-xylene conversion. Effects of pH and calcination temperature were studied, and it was found that pH 8 and 400 °C calcination were optimal conditions. The catalyst (RP-$MnO_x$ (8-400)) showed 100% *o*-xylene conversion to $CO_2$ at 220 °C, 50 °C lower than the catalyst prepared via the conventional precipitation method. This novel method produced materials with 100% $Mn^{4+}$ ion on their surface, whereas the conventional method could only produce materials with 31% $Mn^{4+}$ ion on their surface. It is concluded that that the surface concentration of $Mn^{4+}$ ion plays an important role for its high catalytic activity for the catalytic combustion of *o*-xylene. The open porous hierarchical structure of the α-$MnO_2$ has high BET surface area, may provide more active sites, and facilitate the adsorption and diffusion of reactant molecules. The presence of a small amount of potassium ions in the α-$MnO_2$ channels may weaken the Mn-O bond and promote the reducibility of the catalyst, which also contribute to the excellent catalytic performance of the α-$MnO_2$ material.

This novel synthetic method is environmentally friendly, cost effective and feasible for large scale production of highly active catalyst for the catalytic oxidation of VOCs.

## Acknowledgments

This work was financially supported by the National Natural Science Foundation of China (no.21147004, no.20977024), the Natural Science Foundation of Hebei Education Department (no.2008128, no.Z2010152) and the Foundation of Hebei Normal University (no. L2010Z06). The authors appreciate valuable discussion with Prof. Hong He and experimental help from his group in Research Center for Eco-Environmental Science (RCEES), Chinese Academy of Sciences.

## References

[1] S.Y. Huang, C.B. Zhang, H. He, Catalysis Today 139 (2008) 15.
[2] H.S. Kim, T.W. Kim, H.L. Koh, S.H. Lee, B.R. Min, Applied Catalysis A 280 (2005) 125.
[3] K. Okumura, T. Kobayashi, H. Tanaka, M. Niwa, Applied Catalysis B 44 (2003) 325.
[4] J.C.S. Wu, T.Y. Chang, Catalysis Today 44 (1998) 111.
[5] R.S.G. Ferreira, P.G.P. de Oliveira, F.B. Noronha, Applied Catalysis B 50 (2004) 243.
[6] A.C. Gluhoi, B.E. Nieuwenhuys, Catalysis Today 119 (2007) 305.
[7] S.M. Saqer, D.I. Kondarides, X.E. Verykios, Applied Catalysis B 103 (2011) 275.
[8] M. Chen, X.M. Zheng, Journal of Molecular Catalysis A 221 (2004) 77.
[9] M.A. Alvarez-Merino, M.F. Ribeiro, M.J. Silva, F. Carrasco-Marin, F.J. Maldonado-Hodar, Environmental Science and Technology 38 (2004) 4664.
[10] M.C.M. Alvim-Ferraz, C.M.T.B. Gaspar, Environmental Science and Technology 39 (2005) 6231.
[11] W.B. Li, W.B. Chu, M. Zhuang, J. Hua, Catalysis Today 93–95 (2004) 205.
[12] W.B. Li, J.X. Wang, H. Gong, Catalysis Today 148 (2009) 81.
[13] Y. Liu, M.F. Luo, Z.B. Wei, Q. Xin, P.L. Ying, C. Li, Applied Catalysis B 29 (2001) 61.
[14] T.K. Tseng, H. Chu, H.H. Hsu, Environmental Science and Technology 37 (2003) 171.
[15] C. Lahousse, A. Bernier, P. Grange, B. Delmon,.P. Papaefthimiou, T. Loannides, X. Verykios, Journal of Catalysis 178 (1998) 214.
[16] T.Y. Li, S.J. Chiang, B.J. Liaw, Y.Z. Chen, Applied Catalysis B 103 (2011) 143.
[17] H.J. Li, G.S. Qi, Tana, X.J. Zhang, X.M. Huang, W. Li, W.J. Shen, Applied Catalysis B 103 (2011) 54.
[18] D.A. Aguilera, A. Perez, R. Molina, S. Moreno, Applied Catalysis B 104 (2011) 144.
[19] Y.S. Wu, Y.X. Zhang, M. Liu, Z.C. Ma, Catalysis Today 153 (2010) 170.
[20] Y.S. Wu, M. Liu, Z.C. Ma, S.T. Xing, Catalysis Today 175 (2011) 196.
[21] J.G. Deng, L. Zhang, H.X. Dai, H. He, C.T. Au, Journal of Molecular Catalysis A 299 (2009) 60.
[22] S.T. Xing, R.R. Han, Z.C. Ma, Y.S. Wu, Z.C. Zhou, CrystEngComm 13 (2011) 6033.
[23] J. Carnő, M. Ferrandon, E. Bjőnbom, S. Jaras, Applied Catalysis A 155 (1997) 265.
[24] J. Trawczyński, B. Bielak, W. Mista, Applied Catalysis B 55 (2005) 277.
[25] X.F. Tang, Y.G. Li, X.M. Huang, Applied Catalysis B 62 (2006) 265.
[26] M. Ferrandon, J. Carnö, S. Järas, E. Björnbom, Applied Catalysis A 180 (1999) 141.
[27] P.R. Ettireddy, N. Ettireddy, S. Mamedov, P. Boolchand, P.G. Smirniotis, Applied Catalysis B 76 (2007) 123.
[28] A. Machocki, T. Ioannides, B. Stasinska, W. Gac, G. Avgouropoulos, D. Delimaris, W. Grzegorczyk, S. Pasieczna, Journal of Catalysis 227 (2004) 282.
[29] S. Devaraj, N. Munichandraiah, Journal of Physical Chemistry C 112 (2008) 4406.
[30] J.S. Park, D.S. Doh, K.Y. Lee, Topics in Catalysis 10 (2000) 127.
[31] L. Zhou, J. Zhang, J.H. He, Y.C. Hu, H. Tian, Materials Research Bulletin 46 (2011) 1714.